Angiogenesis
DOI 10.1007/s10456-017-9559-4

ORIGINAL PAPER

Low levels of physiological interstitial flow eliminate morphogen gradients and guide angiogenesis

Venktesh S. Shirure[1] · Andrew Lezia[1] · Arnold Tao[1] · Luis F. Alonzo[2] · Steven C. George[1,3]

Received: 5 March 2017 / Accepted: 30 May 2017

Abstract Convective transport can significantly distort spatial concentration gradients. Interstitial flow is ubiquitous throughout living tissue, but our understanding of how interstitial flow affects concentration gradients in biological processes is limited. Interstitial flow is of particular interest for angiogenesis because pathological and physiological angiogenesis is associated with altered interstitial flow, and both interstitial flow and morphogen gradients (e.g., vascular endothelial growth factor, VEGF) can potentially stimulate and guide new blood vessel growth. We designed an in vitro microfluidic platform to simulate 3D angiogenesis in a tissue microenvironment that precisely controls interstitial flow and spatial morphogen gradients. The microvascular tissue was developed from endothelial colony forming cell-derived endothelial cells extracted from cord blood and stromal fibroblasts in a fibrin extracellular matrix. Pressure in the microfluidic lines was manipulated to control the interstitial flow. A mathematical model of mass and momentum transport, and experimental studies with fluorescently labeled dextran were performed to validate the platform. Our data demonstrate that at physiological interstitial flow (0.1–10 μm/s), morphogen gradients were eliminated within hours, and angiogenesis demonstrated a striking bias in the opposite direction of interstitial flow. The interstitial flow-directed angiogenesis was dependent on the presence of VEGF, and the effect was mediated by αvβ3 integrin. We conclude that under physiological conditions, growth factors such as VEGF and fluid forces work together to initiate and spatially guide angiogenesis.

Keywords αvβ3 integrin · Concentration gradients · Microphysiological systems · Organ-on-a-chip

Introduction

Angiogenesis, the sprouting of vessels from existing vessels, plays an important role in numerous pathophysiological processes, including cancer progression, cardiovascular disease, inflammation, and wound healing [1, 2]. As such, much work has been focused on understanding the molecular mechanisms that initiate and maintain angiogenesis, as well as identifying extracellular pro-angiogenic molecules. Nonetheless, the directional cues guiding angiogenic vessels are less well understood. A mechanistic understanding of directional cues could lead to new therapeutic interventions in a wide range of diseases.

The tissue microenvironment is comprised of cells, extracellular matrix (ECM), and a host of biochemical and biophysical cues that dictate cellular responses. While the biochemical signals are provided by growth factors, cytokines, or chemokines, fluid forces and ECM proteins provide the biophysical signals. Disease can alter both the biochemical and biophysical properties of the tissue microenvironment [3–5]. Interstitial flow and the spatial

Electronic supplementary material The online version of this article (doi:10.1007/s10456-017-9559-4) contains supplementary material, which is available to authorized users.

✉ Steven C. George
scg@wustl.edu

[1] Department of Biomedical Engineering, Washington University in St. Louis, St. Louis, MO 63130, USA

[2] Department of Biomedical Engineering, University of California, Irvine, CA 92697, USA

[3] Department of Energy, Environment, and Chemical Engineering, Washington University in St. Louis, St. Louis, MO 63130, USA

Published online: 12 June 2017

distribution of pro-angiogenic factors are of particular interest in the tumor microenvironment, as the elevation of interstitial flow and vascular endothelial growth factor (VEGF) are both correlated with tumor progression [1, 3]. Interestingly, endothelial cells, stromal cells, and tumor cells, which are the important cell types participating in angiogenesis, can all sense and respond to fluid forces [3, 6–8]. In addition, these same cells can sense pro-angiogenic growth factors, such as VEGF [9, 10].

Angiogenesis involves a series of coordinated cellular events, including cell migration, proliferation, and tube formation [1, 11]. Endothelial cells migrate in response to concentration gradients in assays using single cell type cultures [12, 13]. However, the spatial distribution of a morphogen is strongly coupled in vivo with interstitial flow. For example, interstitial flow distorts the surrounding concentration of tumor-cell-secreted molecules leading to migration of tumor cells along the self-secreted (autocrine) morphogen gradients [14]. Yet, the effect of interstitial flow on concentration gradients in paracrine settings, such as the endothelial cell response to tumor-secreted factors, is poorly understood. We hypothesized that interstitial flow significantly attenuates paracrine concentration gradients, and can independently modulate the direction of angiogenesis.

Advances in microfabrication and microfluidic technology allow the creation of in vitro multicellular microvascular tissues and precise control of microenvironmental factors. Our laboratory has previously developed microfluidic devices to control mass transport and fluid flow to support the development of 3D, interconnected, perfused microvascular networks, as well as to investigate homotypic and heterotypic cell–cell interactions [15–17]. In the current study, we designed a microfluidic device that allows control over spatial concentration gradients and interstitial flow in a vascular microtissue. Our results confirm our hypothesis and demonstrate that low interstitial flow can virtually eliminate spatial morphogen gradients in less than a few hours, and independently guide angiogenesis.

Materials and methods

Cell culture

Normal human lung fibroblasts (NHLF) were obtained from Lonza (Allendale, NJ), and were cultured up to seven passages in complete fibroblast growth medium (FGM; Lonza). Endothelial colony forming cell-derived endothelial cells (ECFC-ECs) were extracted from cord blood as detailed previously [18, 19]. The ECFC-ECs were grown up to seven passages in fully supplemented endothelial growth medium (EGM-2; Lonza).

Cell transduction

The endothelial cells were transduced to constitutively express GFP using pLJM1-EGFP (plasmid # 19319) derived lentiviral transduction particles (Addgene; Cambridge, MA) and polybrene.

Microfabrication

The process of microfabrication is described in detail elsewhere [16]. In short, a master mold of SU8 on a silicon wafer was prepared using photolithography, and then leaching the excess material. The microdevice was created by casting polydimethylsiloxane (PDMS), which was prepared by mixing Sylgard® 184 silicone elastomer base and curing agent (both Dow Corning, Midland, MI) in 10:1 ratio, on the SU-8 master molds. The device design engraved PDMS block was peeled off of the master mold after heat treatment at 60 °C overnight, and then bonded to a flat PDMS sheet using air plasma. The device bonding was cured briefly at 120 °C, and devices were autoclaved prior to use in experiments.

Device design and experimental strategy

The device consists of three tissue chambers and two microfluidic lines running parallel to each other (Fig. 1a, b). The outer microfluidic lines transport nutrients at defined concentrations and pressure by convection. Spatial concentration differences induce diffusive transport through the pores (Fig. 1c). If the pressure is different in the microfluidic lines, transport occurs by convective flow through the tissue channels (interstitial flow). The communication between various chambers was established by micropores, the geometries of which were optimized to avoid leakage of gels into neighboring chambers [15, 16], and yet provide air-bubble-free gel to gel contact between the tissue chambers. In particular, the pore width of 30 μm and length of 55 μm produced leak-proof, bubble-free interfacing of the gels. The devices were designed with the same number of communication pores between the tissue chambers and the fluidic lines to facilitate formation of near linear concentration and pressure gradients across the length of the tissue chambers.

The strategy for the assays was to create a 3D vascular network in the central chamber and fill the side tissue chambers with acellular fibrin gels, which serve as observation chambers (Fig. 1c, d). The flow in the microfluidic lines was maintained by a hydrostatic pressure drop created by differential levels in the source and sink from each line. The concentration gradient in the absence of interstitial flow (diffusion dominant) was created by maintaining the two microfluidic lines at different concentrations, but the

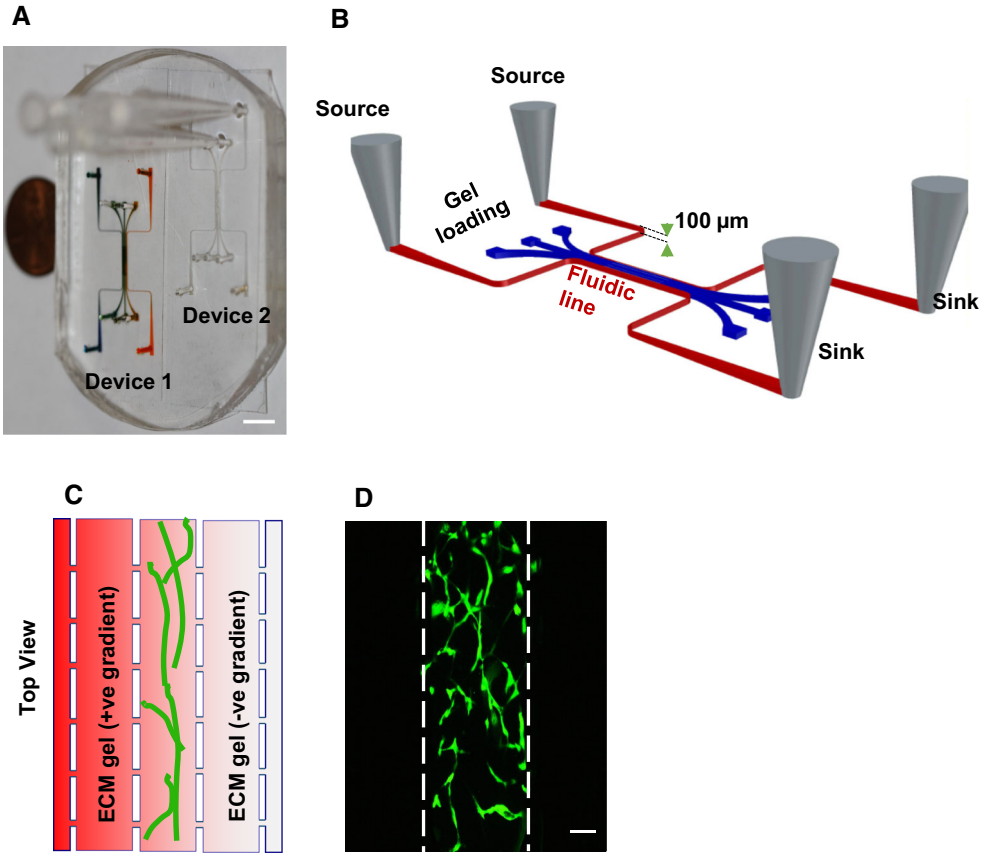

Fig. 1 Schematic diagram of the microfluidic device. **a** PDMS platform with two devices. Device on the left has been filled with colored dye to highlight the microfluidic channels. The *scale bar* indicates 3 mm. **b** The device consists of three tissue chambers (*blue*) and two microfluidic lines (*red*) connected to sources and sinks. Small communication pores (30 µm minimum diameter) allow the microfluidic lines and tissue chambers to communicate via diffusion and convection of interstitial fluid. **c** The vascular tissue is created in the central chamber while the side chambers are loaded with ECM gels. The pressure and concentration gradients can be created by maintaining differential concentration or pressure in the fluidic lines. If a molecule or morphogen is added to the microfluidic line on the *left side*, the central tissue experiences a positive (+ve) gradient (increasing concentration) on *left side* and negative (−ve) (decreasing concentration) on the *right side* indicated by *red color* gradient from left to right. **d** Two days after the device is loaded with endothelial cells and fibroblasts, the endothelial cells form a network of vessel (*Green*) in the central chamber. *Scale bar* shows 100 µm

same average hydrostatic pressure. Maintaining a differential in the average pressure in the two microfluidic lines created interstitial flow through the tissue.

Device loading, tissue growth, and tissue treatments

The microtissue construct was created from 1:2 mixture of ECFC-ECs and NHLFs to produce a final concentration of 10 and 20 million cells/ml, respectively, in a fibrin gel. The fibrin gel was prepared by mixing bovine fibrinogen (Sigma-Aldrich, St. Louis, MO) at 10 mg/ml and bovine plasma thrombin (Sigma-Aldrich) at 50 U/ml to produce a final thrombin concentration of 3 U/ml. Acellular fibrin gel (without cells) was first introduced in the side tissue chambers, followed by a cellularized fibrin gel into the central tissue compartment (Fig. 1d). After 30 min, media were introduced through the microfluidic lines. The vascular network was developed with complete EGM2 media under nominal interstitial flow, maintained by an average pressure gradient of 2 mm H_2O, in either direction for 24 h [15, 17]. The tissue chamber was then exposed to a specified spatial concentration gradient and/or interstitial flow. In some experiments, the microtissues were grown for 2 days and then treated with Cilengitide (1 or 10 µM, Sigma-Aldrich) or azide-free anti-human αvβ3 (LM609) monoclonal antibody (mAb; EMD Millipore, Billerica, MA) at 15 µg/ml.

Device staining and imaging

All labeling reagents were first introduced on one side of the device in a microfluidic line with an average hydrostatic pressure of 25 mm of H_2O, while keeping the other side near zero mm H_2O. This condition induces interstitial flow across the microtissue. Subsequently, the direction of

the interstitial flow was reversed for a similar amount of time.

Following an experiment, the microtissues were first fixed with 10% formaldehyde. The tissues were labeled by endothelial cell-specific anti-human CD31 mAb (Dako, Glostrup, Denmark) or anti-human αvβ3 mAb, and subsequently stained with AlexaFluor conjugated secondary antibody. Finally, the microtissues were stained with DAPI to visualize nuclei. The microtissues were imaged under wide field fluorescence using an IX 83 motorized inverted microscope (Olympus, Tokyo, Japan) or FV1200 Fluoview biological confocal laser scanning microscope (Olympus) connected to computers with MetaMorph Advanced (version 7.8.2.0) or FV10-ASW image acquisition and analysis software (both Olympus). As required, the image analysis was also performed using ImageJ 1.47 V and AngioTool (version 0.5a). The vessel density was calculated as total vessel length per area (μm/mm^2).

Finite element simulations

The finite element analysis was performed using COMSOL Multiphysics® 5.2a software. The convection–diffusion equations of mass and momentum transport were solved to find concentration gradients under interstitial flow conditions. The solutions were obtained in COMSOL using fluid flow through porous media and transport of diluted species modules with incompressible, single-phase, laminar flow characteristics.

The computer aided design (CAD) file used for microfabrication of the device was imported into COMSOL as an object geometry. The no-slip boundary condition was used for all surfaces except the microfluidic entrance and exit. The hydrostatic pressure heads in the source and sink drove the flow in the microfluidic lines. The pressure and velocity fields were used to interpret the magnitude and pattern of convection and diffusion. To estimate fluid flow around a microvessel in the microfluidic device, a hypothetical vessel of diameter 50 μm was created in the central chamber of the tissue using AutoCAD. The hydraulic conductivity of the vascular wall was assumed to be equal to the previously reported value for human umbilical cord endothelial cell in vitro cultures (2.9×10^{-6} cm s^{-1} cm-H_2O^{-1}) [20]. The fluid flow through a unit length of the vessel was found my multiplying the average velocity through the vessel wall by ($\pi D/2$), where D is diameter of the vessel. The fluid flow per unit length (along y-axis) of the device was found by multiplying the average fluid velocity in the ECM (non-vessel area) with the height of the chamber (100 μm).

We also performed simulations on a hypothetical tissue of similar dimensions to the microfluidic device. We utilized the same width (1 mm) for the tissue as that in the device as this is similar to the distance that separates capillaries in vivo [36]. We increased the height or length (100 mm) to simply reduce the edge effects. A microvessel of equal length and 50 μm in diameter was created on the right boundary of the tissue, similar to the microfluidic line on the right side of the device. At the beginning of the simulations (time = 0), the concentration within the tissue was zero. The left boundary of the tissue was set at finite concentration (source of pro-angiogenic factors, e.g., tumor, or the left microfluidic line), and the transport out of the tissue was from the right boundary into the microvessel. The microvessel fluid velocity was set at a physiological value of 500 μm/s [21, 22], unless otherwise described. The zero concentration and no diffusive flux were used as boundary conditions for the microvessel inlet and outlet, respectively.

The following values for physical constants were used in the simulations: diffusion coefficient of dextran, 7×10^{-11} m^2/s; porosity and hydraulic permeability of fibrin gel, 0.99 and 1.5×10^{-13} m^2, respectively [16, 23]; the dynamic viscosity at 25 °C and density of water, 0.89 cP and 1000 kg/m^3, respectively; the diffusion coefficient of VEGF, 10^{-11} m^2/s.

Fluorescence recovery after photo bleaching (FRAP)

Fluorescent recovery after photobleaching (FRAP) was used to experimentally measure the interstitial flow rate [24]. All tissue compartments of the device were loaded with acellular fibrin gel. FITC-dextran (70 kDa, Sigma-Aldrich) was added to the fluidic lines and pressure gradients of 10 and 20 mm H_2O were created across the tissue chamber. FRAP was then performed on the device at the center of central tissue chamber using a confocal microscope (Zeiss LSM 700, Carl Zeiss AG, Feldbach, Switzerland). A circular region of 30 μm was bleached, and images were acquired for a total of 30 s. The images were individually marked for the bleached region using the circle tool in ImageJ, and the coordinates of centroid of the region were found. The distance travelled by the centroid of the bleached spot in a given time was calculated to find convective velocity of fluid flow in the device [24].

Statistics

Statistical analysis was performed using t test or one-way ANOVA and Tukey test for multiple comparisons. All data are presented as the mean ± standard error. Results were considered statistically significant for $p < 0.05$.

Results

Angiogenesis is directed by a morphogen gradient in the absence of interstitial flow

To demonstrate the effect of a controlled morphogen gradient, 3D vascular networks were prepared for 2 days. During this period, the endothelial cell growth was restricted to the central compartment, and no migration was observed into the side tissue compartment (Fig. 1d). The vascular tissues were then exposed to a linear gradient of VEGF under zero interstitial flow conditions. Under zero concentration gradient (mean VEGF concentration of either zero or 2 ng/ml), the vessel network development was primarily restricted to the central tissue compartment (Figs. 2a, 4d), with no bias toward either side compartment. To study the effect of a soluble VEGF gradient, we used the VEGF 121 isoform, which has less binding affinity for fibrin [25]. There is a striking bias of vessel sprouting toward positive gradients (i.e., toward an increasing concentration) of VEGF, compared to zero or a negative gradient as indicated by a dramatic increase in the vessel density in the +ve gradient chamber (Fig. 2b, c). We defined bias of angiogenic sprouting as the ratio of the vessel sprouting into a gradient chamber to the total vessel sprouting into both side chambers. The bias of angiogenesis along the positive concentration gradient was more than 80% for the concentration gradient conditions.

Interstitial flow eliminates spatial morphogen gradient

The analysis of concentration gradients under normal and pathological flow conditions was performed in COMSOL on a hypothetical tissue. The Peclet number (*Pe*) provides an estimate of convective to diffusive mass transport and is defined as follows,

$$\mathrm{Pe} = \frac{ul}{D} \tag{1}$$

where u is the velocity of fluid (m/s), l is length (m), and D is the diffusion coefficient (m^2/s). It can also be convenient to consider *Pe* as a dimensionless convective velocity (proportional to u). For VEGF ($D = 10^{-11}$ m^2/s) and distance (l) = 1 mm, the range of *Pe* for normal tissue ($0.1 < u < 10$) [26] is 10–1000. When no flow exists in our hypothetical tissue (or device), a linear concentration gradient represents the steady state (Fig. 3a). When the lowest flow (0.1 μm/s or $Pe = 10$) is initiated from left to right, the morphogen (VEGF) is convected to the right and the concentration gradient is eliminated over the vast majority of the width within 6 h (Fig. 3b). When $Pe = 20$ (0.2 μm/s), the gradient is eliminated more rapidly (Fig. 3c).

To experimentally determine the impact of interstitial flow, we first measured the flow velocity using FRAP. The displacement of the centroid of the bleached spot was tracked over time in the FRAP videos to determine the convective velocity (Fig. 3d). Pressure gradients of 10 and 20 mm H_2O across the tissue created steady interstitial fluid velocities of 12 ± 1 and 43 ± 5 μm/s, respectively. When these experimental measurements were statistically compared with the COMSOL values no significant difference was found (Fig. 3e). Thus, the interstitial fluid velocity can be easily controlled and altered by simply altering the hydrostatic pressure in the reservoir.

To demonstrate the impact of interstitial flow on the concentration gradient in the device, 70 kDa FITC labeled dextran was perfused through one fluidic line while buffer

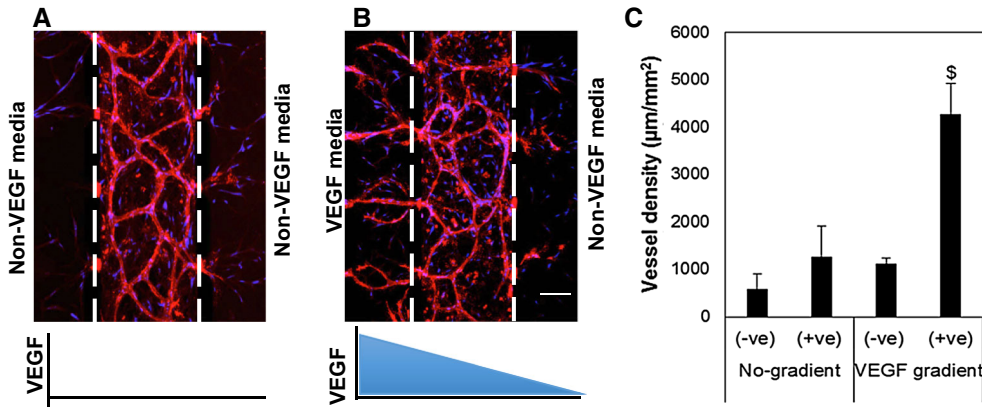

Fig. 2 Vessels are guided by VEGF gradient under diffusion condition. **a**, **b** The devices were maintained from day 2 up to 10 days under non-gradient (**a**) and gradient (**b**) conditions and were stained with endothelial specific CD31 (*red*) and DAPI (*blue*). The concentration gradient of VEGF was created by 2 ng/ml VEGF media (*left side*) and non-VEGF media (*right side*). **c** The image analysis was performed to quantify vessel density in the gradient chambers. $Indicates statistically significant with respect to the −ve gradient chamber and non-gradient conditions. *Scale bar* shows 100 μm

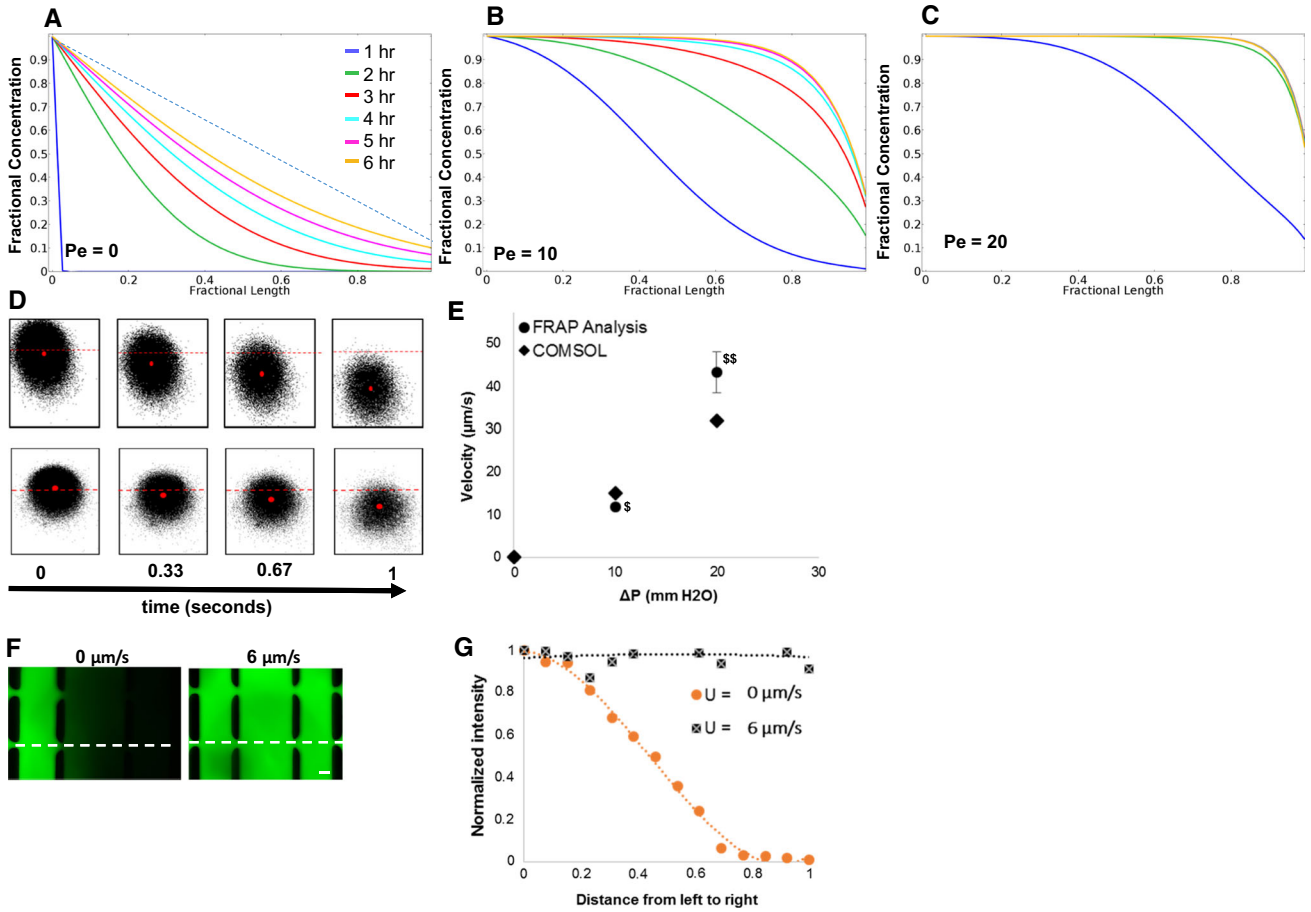

Fig. 3 Concentration gradients are washed away under interstitial flow. **a–c** The concentration profiles of morphogens (VEGF) in a hypothetical tissue (similar dimensions to the microfluidic device, see text) were calculated by the mathematical model at progressively increasing values of the *Pe* number: **a** $Pe = 0$; **b** $Pe = 10$; **c** $Pe = 20$. An interstitial flow of fluid with morphogen was created from left to right in the tissue. The tissue compartment initially ($t = 0$) had no morphogen. The concentrations were determined along a horizontal line running at the vertical center of the tissue. The *Pe* number was varied by increasing interstitial flow velocity 0–0.2 μm/s. The dotted line in (**a**) shows the steady state concentration gradient under no-flow ($Pe = 0$) condition. **d** FRAP analysis was performed to experimentally determine the interstitial flow velocity in the device. The centroid (*red dot*) of the bleached spot is tracked by acquiring time lapse images. The time lapse sequence images shown on top and bottom are, respectively, for 20 and 10 mm H_2O pressure gradient across the tissue chamber. The images from left to right were acquired at 0, 0.33, 0.67, and 1 s, respectively. *Red dashed line* is fixed and represents the position of the centroid at time = 1. **e** The velocities were calculated from FRAP analysis and COMSOL simulations at various pressure gradients. $^{\$}$,$^{\$\$}$Indicate statistically significant with respect to ΔP (experimental). **f** Various interstitial flow velocities were created by varying the pressure gradient, and the concentration profile of 70 kDa dextran labeled with FITC (*top panels*) was imaged after 2 h. **g** The intensity of dextran-FITC was measured at various points (*dotted line* in **f**) in the tissue chamber and normalized with the fluidic line intensity of the dextran-FITC at various pressure gradients. *Scale bar* shows 100 μm

was perfused through the other fluidic line. The molecular weight of the dextran was similar in magnitude to the molecular weight of VEGF (40 kDa). As expected, the slope of the concentration gradient decreased with increasing interstitial flow. In particular, at 5 mm H_2O pressure gradient, which created a velocity of about 6 μm/s (Fig. 3f), the concentration gradient of dextran was completely eliminated and a flat concentration profile of dextran was obtained within 1 h (Fig. 3f, g), consistent with the theoretical simulations.

Vessel sprouting and migration is against the direction of interstitial flow

We next tested whether interstitial flow could independently stimulate and guide angiogenesis. When the vessels were exposed to interstitial flow of approximately 6 μm/s, biased vessel sprouting in the upstream chamber compared to downstream chamber was observed, but only when VEGF was present (2 ng/ml; Fig. 4a–c). The vessels in the central chamber and the sprouting vessels in the upstream

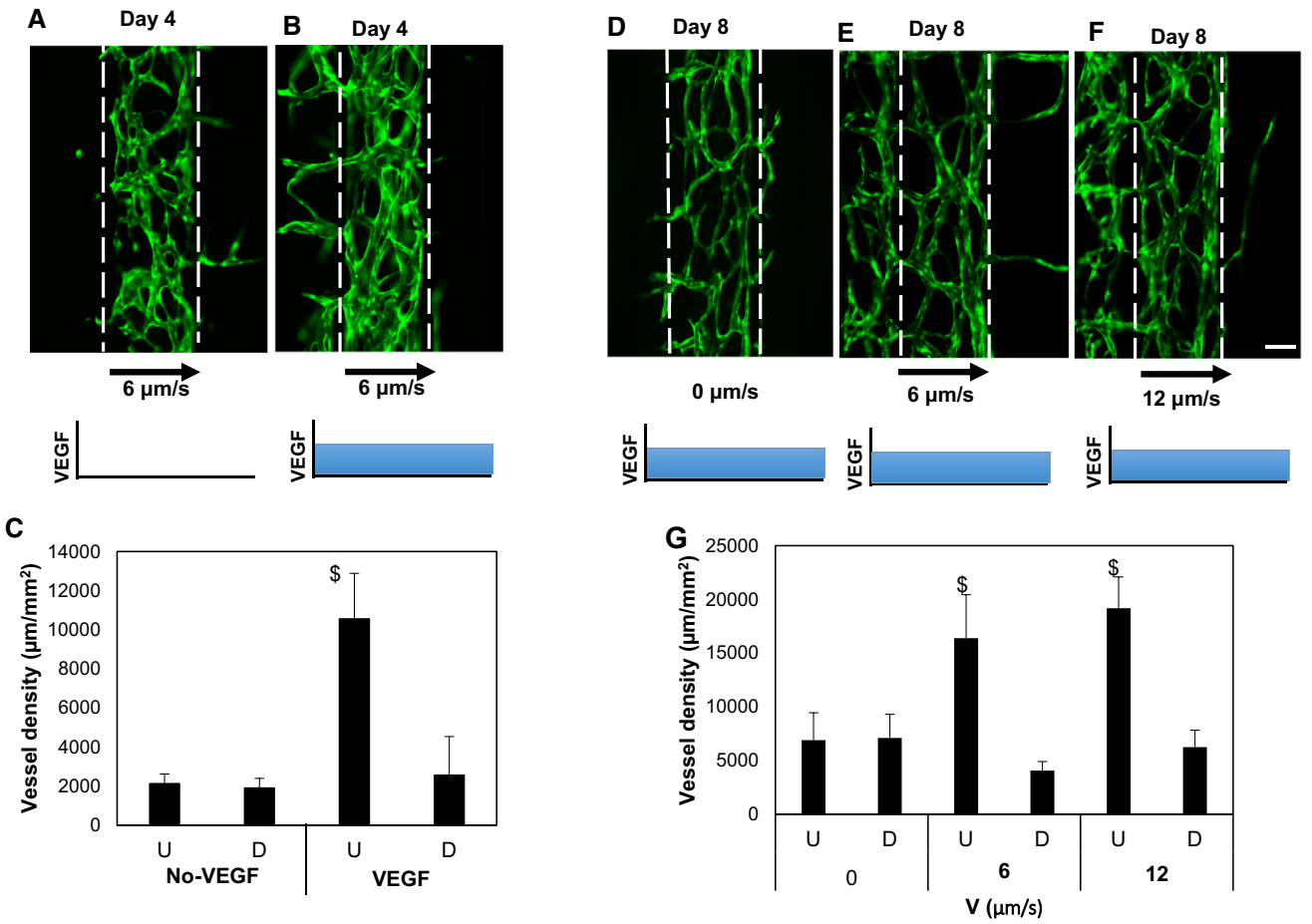

Fig. 4 VEGF is required for interstitial flow-directed sprouting of the vessels. **a–f** On day zero, mixture of ECFC-ECs (GFP; *green*) and NHLF in fibrin gel was seeded in the central tissue chamber and the other two tissue compartments were filled with fibrin gel. The devices were maintained with or without VEGF (2 ng/ml) in EGM culture media from day 2 to indicated number of days. The interstitial flow was created by maintaining high hydrostatic pressure in the left fluidic line, which resulted into the indicated flow velocities and flow direction. *Scale bar* shows 100 µm. **c**, **g** The image analysis was performed to quantify the vessel length in upstream and downstream chambers, indicated by *U* and *D*. **c** $Indicates statistically significant with respect to the downstream chamber and with respect to the no-VEGF condition. **g** $Respect to the downstream chamber and with respect to the no-flow condition

chamber have clear lumens (Fig. S1). To test whether the magnitude of interstitial flow affects the magnitude of angiogenesis, we repeated the experiments at 0, 6, and 12 µm/s and measured the vessel network at day 8. In the absence of interstitial flow, there was no bias of sprouting through 8 days (Fig. 4d, g). As at day 4, interstitial flow significantly biased vessel sprouting in the upstream chamber compared to downstream chamber at day 8 (Fig. 4d–f). However, the magnitude of interstitial flow did not significantly impact the magnitude of vessel growth (Fig. 4g) or the directional bias of angiogenesis, which remained more than 80% for both interstitial flow conditions. We also found that there was no significant bias in stromal cell migration due to interstitial flow (Fig. S2).

To analyze the effect of transient morphogen gradients at the beginning, we created concentration gradient and interstitial flow conditions simultaneously. Maintaining the same (zero concentration gradient) or different concentrations (finite concentration gradient) of VEGF in the fluidic lines created no gradient or short (<1 h) transient gradients, respectively. The unsteady state concentration gradient lasts for <1 h, after which the gradient was washed away (Fig. S3A), and angiogenesis in the upstream chamber was not impacted by an early spatial gradient in VEGF (Fig. S3B and C).

We tested whether the vessels created in the device resemble the permeability of in vivo vessels, we tested the barrier function of the vessels using 70 kDa dextran, which served as a surrogate for pro-angiogenic growth factors such as VEGF (MW 40 kDa). The fluorescent microscopy results suggest that the vessels formed in the device serve as a barrier to large molecules (Fig. S4) and the model results suggested that the majority of fluid flow passes around (as opposed to through) the vessels (Fig. S5).

Finally, we tested effect of matrix stiffness by creating vascular tissues in soft (2 mg/ml fibrinogen) and stiff (10 mg/ml fibrinogen) ECMs. We have previously demonstrated that the compressive modulus of fibrin increases >fivefold when the fibrin concentration increases from 2.5 mg/ml to 10 mg/ml [27], and that vessel network formation and sprouting is enhanced in softer gels [27, 28]. The interstitial flow bias of angiogenesis in the soft ECM was smaller (<71%) than in stiff matrix (>80%; Fig. S6A and B). Also, the number of sprouts was higher in the soft matrix than in the stiff matrix (Fig. S6C). These data suggest that a soft ECM facilitates sprouting, but that the directional bias of angiogenesis created by interstitial flow is improved in stiff matrix.

Interstitial flow-directed angiogenesis is mediated by αvβ3 integrin

As interstitial flow can independently guide angiogenic growth, we next sought to determine whether integrins mediate this phenomenon. The integrins αvβ3 and αvβ5 bind to fibrin, the main component of the ECM in our microfluidic device, and these integrins are also associated with tumor angiogenesis and mechanotransduction [29–32]. To determine the potential molecular mediators of interstitial flow driven angiogenesis, we chose to analyze the effect of these integrins under an interstitial flow velocity of 12 μm/s, in the absence of morphogen gradients. When the microvascular tissue was treated with Cilengitide, a well-known small molecule inhibitor of αvβ3 and αvβ5 integrins [33], the angiogenic sprouting in the upstream chamber was significantly reduced compared to the control conditions (Fig. 5b, c, e). The αvβ3 integrin is of particular interest as it has been considered an important target for tumor angiogenesis [31]. To investigate whether the reduction in angiogenesis is primarily due to αvβ3, the tissues were treated with a function blocking mAb against αvβ3. The endothelial cells and stromal fibroblasts in the microvascular tissue both expressed αvβ3 integrin (Fig. 5a) (isotype control was negative, data not shown). The antibody treatment significantly reduced the angiogenic sprouting in the gradient chamber, compared to untreated microvascular tissue (Fig. 5b, d, e).

Discussion

Angiogenesis is part of both normal (e.g., wound healing, exercise) and abnormal (e.g., cancer) biology, and is thus an attractive target for therapeutic interventions. Wound healing, cardiovascular diseases, and cancer can all impact interstitial flow and secretion of pro-angiogenic growth factors [1, 2]. Fluid forces not only impact cell behavior, but can also profoundly impact spatial concentration gradients. We hypothesized that interstitial flow could significantly attenuate spatial morphogen gradients and independently provide directional cues for angiogenesis. Our simple microfluidic platform supports the development of 3D microvascular networks, and provides control over interstitial flow and spatial concentration gradients. Our results demonstrate that interstitial flow can virtually eliminate spatial gradients, even at the lowest physiological level of interstitial flow within hours and can independently provide directional cues for angiogenesis that are mediated, in part, by αvβ3 integrin.

The transport of molecules within interstitial tissue is governed primarily by diffusion and convection. Diffusion and convection occur simultaneously in vivo, and their relative impact on the transport of morphogens depends on their relative magnitude. The interstitial flow (velocity) is altered in disease states, and has been reported to be as high as 150 μm/s in the tumor microenvironment [34]. In contrast, interstitial flow in most normal tissues is between 0.1 to 10 μm/s [23, 35]. The *Pe* is a convenient dimensionless number that captures the ratio of convection to diffusion. Even at the lowest physiological interstitial flow (~0.1 μm/s), *Pe* for VEGF over a 1 mm distance is approximately 10. We demonstrated both theoretically and experimentally (with dextran) that over a wide range of interstitial flows, including the lowest flow, the spatial gradient of a large molecular weight protein is virtually eliminated. The magnitude of flow only impacts the rate at which the gradient dissipates. Two conditions exist which could impact these findings. First, if a protein binds to the ECM, it cannot be so easily washed away. This is, in fact, the case of larger molecular weight VEGF (e.g., VEGF165) which is present in vivo. In this case, however, the spatial gradient (ECM-bound gradient) may not be sustained long if the ECM saturates due to continuous convection of morphogens. Second, a short steep gradient near the sink (right boundary of simulations in Fig. 3a–c) exists, which is increased in magnitude if the capillary flow is increased (Fig. S7). Nonetheless, these data suggest that concentration gradients of soluble morphogen are severely attenuated under the influence of interstitial flow.

When the microvasculature was exposed to interstitial flow, sprouting was strongly biased against the direction of interstitial flow (upstream), compared with the direction of interstitial flow (downstream). However, this observation only occurred in the presence of a low concentration of VEGF (2 ng/ml). This result suggests that, while angiogenesis can be guided or directed by interstitial flow alone, the endothelial cell must be in an activated state (e.g., in the presence of VEGF) in order to respond to flow. In other words, when combined with our observations that low interstitial flow can eliminate spatial gradients of soluble

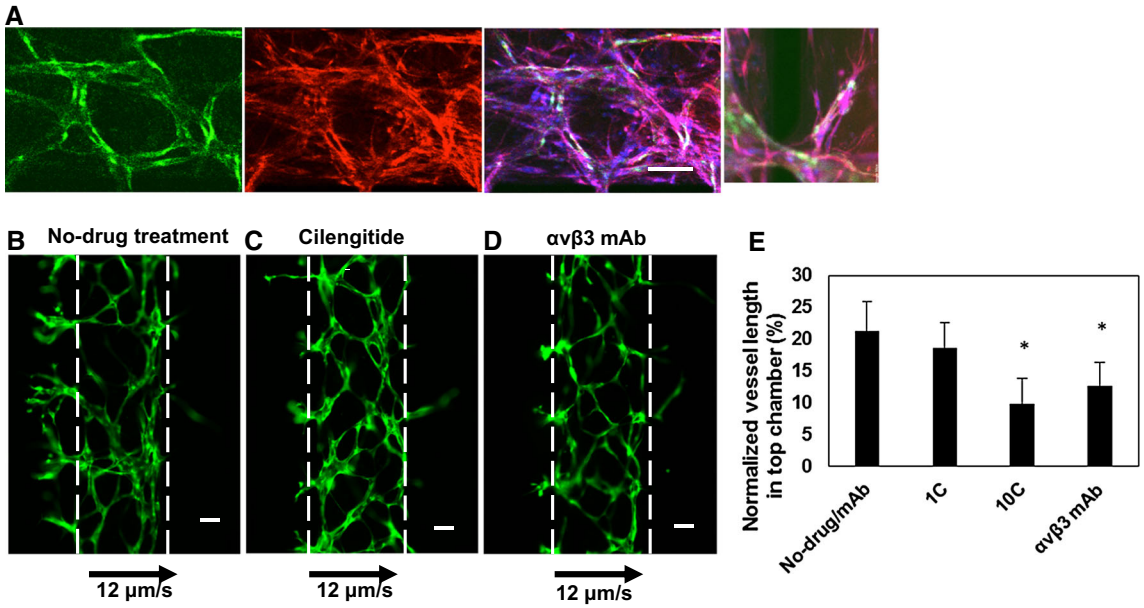

Fig. 5 Interstitial flow-directed angiogenesis is mediated by αvβ3 integrins. **a** The vasculature was grown in the microfluidic device and stained with DAPI (*blue*), αvβ3 mAb (*red*). The endothelial cells were GFP transduced (*green*). The *scale bar* indicates 100 μm. **b–d** The vasculature was grown for 2 days and treated with Cilengitide (10 μM) or αvβ3 mAb containing medium for 4 days and non-drug treated vasculature served as a control. The direction of flow and velocity is as indicated. *Scale bar* shows 100 μm. **e** The image analysis was performed to quantify the vessel length in top chamber and normalized with total vessel length in the device 4 days' post-treatment. 1C and 10C indicate 1 and 10 μM Cilengitide concentrations. *Indicates statistically significant with respect to untreated control

molecules, our data suggest that a paradigm for directed angiogenesis begins with activation by a pro-angiogenic morphogen such as VEGF, but that the resulting vessel growth is guided or directed by fluid flow. This paradigm suggests that morphogens and physical forces work in concert to direct new blood vessels to the source of interstitial flow (e.g., a neighboring functional capillary network), and contrasts with the more commonly held concept that morphogen gradients alone direct new blood vessel growth [36–38].

Angiogenesis follows a complex series of events, which includes endothelial cell migration, proliferation, and tube formation [11]. Neighboring stromal cells secrete factors necessary to support various critical steps involved in angiogenesis, in particular tube formation and stabilization. It has been demonstrated that normal human lung fibroblasts produce factors necessary to support formation of endothelial tubes with hollow lumens [17, 39, 40]. Our laboratory has previously demonstrated the development of microvessels using cord blood derived endothelial cells and lung fibroblasts in microfluidic platforms [16, 17], and since then several other reports have used similar systems [41–43]. The permeability of these capillaries (4.5×10^{-9} m/s for 70 kDa dextran) is close to in vivo capillaries [44]. The averaged permeability of the tumor microvessels (10^{-8} m/s for 70 kDa [45]) is higher than that of microvessels in our system, but the leakiness of individual tumor microvessels is widely variable, ranging from hyperpermeable to non-leaky microvessels [46]. Furthermore, the capillaries formed from co-culture of lung fibroblasts and endothelial cells anastomose with in vivo microvasculature and become perfused with blood when implanted in mice [19]. This co-culture system provides a more physiological alternative, compared to assays using only endothelial cells [6, 12, 13, 47–50] to mimic in vivo angiogenesis. Moreover, the physical dimensions, such as the diameter, of the microvasculature formed by our assay resemble that of the in vivo microvasculature (<50 μm). Previously reported microdevices for angiogenesis assays consist of microvessels created by coating microchannels with endothelial cells resulting in large diameter (>100 μm) endothelial cell-lined tubes [12, 13, 48, 49]. Additionally, the microvessels in our system are circular in cross section (Fig. S1), which reduces artifacts caused in non-circular morphologies; for instance, rectangular microvessels have been shown to sprout mainly at the corners of the vessel [48]. Nonetheless, the microvessels in our systems did not experience intraluminal shear stress at the level of in vivo microvessels, which could affect the rate of growth of the vessels.

To validate our platform, we created concentration gradients of VEGF using a biologically relevant concentration of VEGF, 2 ng/ml [51]. The concentration gradient produced vessel sprouts biased strongly in the direction of positive concentration gradients compared to the negative

gradient. This observation is consistent with other reports that have shown that endothelial cells migrate in the direction of the positive concentration gradient [12, 49]. Thus, the results demonstrate that under diffusion dominant conditions angiogenesis can be directed by spatial concentration gradients of morphogens.

Previously, interstitial flow passing through the vascular wall (transmural) has been found to facilitate angiogenesis [6, 52, 53] in the upstream direction [6, 52]. On the other hand, interstitial flow passing around endothelial cells, embedded in VEGF linked ECM, has been found to bias sprouting in downstream direction by amplifying gradients of VEGF liberated by proteases [54]. Furthermore, a recent report showed that cancer cells migrate against the direction of flow by sensing higher tension on the upstream side of cells via β1-integrin adhesion complexes and by activating focal adhesion proteins on the upstream side of cell membrane [7]. The interstitial flow in our 3D network of vessels mainly passes around the vessel (abluminal; Fig. S3 and S4), thus applying fluid forces on the abluminal side of the vessels. We found that αvβ3 integrin mediates angiogenic sprouting of the vessels in the upstream direction of fluid flow. This is consistent with αvβ3 integrin as a mechanotransducer [32] and observations that integrins, in general, impact cellular functions [55] required for angiogenesis. This finding is also consistent with a previous study which reported that flow induces angiogenesis through focal adhesion kinase (FAK) mediated signaling which is associated with integrin signal transduction [53]. While it is likely that the αvβ3 integrins expressed on endothelial cells trigger sprouting and directed growth of new vessels in response to interstitial flow, we cannot rule out a role of fibroblasts, which are present in our culture systems and also express the αvβ3 integrin. It is significant to note that αvβ3 integrins are targeted to reduce angiogenesis in cancer treatments [30, 31]. Our data suggest that this integrin plays a role in sensing interstitial flow to direct sprouting of vessels.

We also found that soft matrix facilitates angiogenesis but the directional bias of angiogenesis is more in stiff matrix (Fig. S6). Interestingly, it has been shown that sprouts align along a VEGF gradient more readily in stiff than in soft ECM [56]. These data indicate that microvessel sprouts better sense the directional cues in stiff than soft matrix, but further studies are warranted to uncover the molecular mechanism.

In conclusion, we have presented a microfluidic platform with a 3D microvessel network that is particularly adept at investigating how interstitial flow and morphogen gradients can initiate and guide angiogenesis; however, the platform could also be used to study a range of biological phenomenon that are impacted by cell migration, concentration gradients, and interstitial flow. We show that low physiological levels of interstitial flow can significantly attenuate concentration gradients of soluble morphogens, and that these same levels of low flow can guide or direct angiogenic sprouting that is mediated in part by αvβ3 integrin. Our results suggest that chemical gradients (growth factors) and mechanical (fluid forces) forces work together to initiate and guide vessel sprouting, respectively.

Acknowledgements This work was supported by grants from the National Institutes of Health (UH3 TR00048, R01 CA170879, and F31 CA163049). We would like to thank Mr Vinson Tran, Mo Kebaili, Linda McCarthy (University of California, Irvine) and Sandra Lam (Washington University in St. Louis) for technical assistance. We would also like to thank Dr. Abraham Lee for helpful advice and material assistance during the development stages of this project.

References

1. Carmeliet P, Jain RK (2000) Angiogenesis in cancer and other diseases. Nature 407(6801):249–257. doi:10.1038/35025220
2. Khurana R, Simons M, Martin JF, Zachary IC (2005) Role of angiogenesis in cardiovascular disease: a critical appraisal. Circulation 112(12):1813–1824. doi:10.1161/CIRCULATIONAHA.105.535294
3. Swartz MA, Lund AW (2012) Lymphatic and interstitial flow in the tumour microenvironment: linking mechanobiology with immunity. Nat Rev Cancer 12(3):210–219. doi:10.1038/nrc3186
4. Roussos ET, Condeelis JS, Patsialou A (2011) Chemotaxis in cancer. Nat Rev Cancer 11(8):573–587. doi:10.1038/nrc3078
5. Wiig H, Swartz MA (2012) Interstitial fluid and lymph formation and transport: physiological regulation and roles in inflammation and cancer. Physiol Rev 92(3):1005–1060. doi:10.1152/physrev.00037.2011
6. Song JW, Munn LL (2011) Fluid forces control endothelial sprouting. Proc Natl Acad Sci USA 108(37):15342–15347. doi:10.1073/pnas.1105316108
7. Polacheck WJ, German AE, Mammoto A, Ingber DE, Kamm RD (2014) Mechanotransduction of fluid stresses governs 3D cell migration. Proc Natl Acad Sci USA 111(7):2447–2452. doi:10.1073/pnas.1316848111
8. Shi ZD, Tarbell JM (2011) Fluid flow mechanotransduction in vascular smooth muscle cells and fibroblasts. Ann Biomed Eng 39(6):1608–1619. doi:10.1007/s10439-011-0309-2
9. Goel HL, Mercurio AM (2013) VEGF targets the tumour cell. Nat Rev Cancer 13(12):871–882. doi:10.1038/nrc3627
10. Turner N, Grose R (2010) Fibroblast growth factor signalling: from development to cancer. Nat Rev Cancer 10(2):116–129. doi:10.1038/nrc2780
11. Jain RK, Schlenger K, Hockel M, Yuan F (1997) Quantitative angiogenesis assays: progress and problems. Nat Med 3(11):1203–1208
12. Bischel LL, Young EW, Mader BR, Beebe DJ (2013) Tubeless microfluidic angiogenesis assay with three-dimensional endothelial-lined microvessels. Biomaterials 34(5):1471–1477. doi:10.1016/j.biomaterials.2012.11.005
13. Zheng Y, Chen J, Craven M, Choi NW, Totorica S, Diaz-Santana A, Kermani P, Hempstead B, Fischbach-Teschl C, Lopez JA, Stroock AD (2012) In vitro microvessels for the study of angiogenesis and thrombosis. Proc Natl Acad Sci USA 109(24):9342–9347. doi:10.1073/pnas.1201240109
14. Shields JD, Fleury ME, Yong C, Tomei AA, Randolph GJ, Swartz MA (2007) Autologous chemotaxis as a mechanism of

tumor cell homing to lymphatics via interstitial flow and autocrine CCR7 signaling. Cancer Cell 11(6):526–538. doi:10.1016/j.ccr.2007.04.020
15. Alonzo LF, Moya ML, Shirure VS, George SC (2015) Microfluidic device to control interstitial flow-mediated homotypic and heterotypic cellular communication. Lab Chip 15(17):3521–3529
16. Hsu YH, Moya ML, Abiri P, Hughes CC, George SC, Lee AP (2013) Full range physiological mass transport control in 3D tissue cultures. Lab Chip 13(1):81–89. doi:10.1039/c2lc40787f
17. Moya ML, Hsu YH, Lee AP, Hughes CC, George SC (2013) In vitro perfused human capillary networks. Tissue Eng Part C Methods 19(9):730–737. doi:10.1089/ten.TEC.2012.0430
18. Melero-Martin JM, Khan ZA, Picard A, Wu X, Paruchuri S, Bischoff J (2007) In vivo vasculogenic potential of human blood-derived endothelial progenitor cells. Blood 109(11):4761–4768. doi:10.1182/blood-2006-12-062471
19. Chen X, Aledia AS, Popson SA, Him L, Hughes CC, George SC (2010) Rapid anastomosis of endothelial progenitor cell-derived vessels with host vasculature is promoted by a high density of cotransplanted fibroblasts. Tissue Eng Part A 16(2):585–594. doi:10.1089/ten.TEA.2009.0491
20. Luckett PM, Fischbarg J, Bhattacharya J, Silverstein SC (1989) Hydraulic conductivity of endothelial cell monolayers cultured on human amnion. Am J Physiol 256(6 Pt 2):H1675–H1683
21. Nuttall AL (1987) Velocity of red blood cell flow in capillaries of the guinea pig cochlea. Hear Res 27(2):121–128
22. Ivanov KP, Kalinina MK, Levkovich YuI (1981) Blood flow velocity in capillaries of brain and muscles and its physiological significance. Microvasc Res 22(2):143–155
23. Swartz MA, Fleury ME (2007) Interstitial flow and its effects in soft tissues. Annu Rev Biomed Eng 9:229–256. doi:10.1146/annurev.bioeng.9.060906.151850
24. Jain RK, Stock RJ, Chary SR, Rueter M (1990) Convection and diffusion measurements using fluorescence recovery after photobleaching and video image analysis: in vitro calibration and assessment. Microvasc Res 39(1):77–93
25. Martino MM, Briquez PS, Ranga A, Lutolf MP, Hubbell JA (2013) Heparin-binding domain of fibrin(ogen) binds growth factors and promotes tissue repair when incorporated within a synthetic matrix. Proc Natl Acad Sci USA 110(12):4563–4568. doi:10.1073/pnas.1221602110
26. Rutkowski JM, Swartz MA (2007) A driving force for change: interstitial flow as a morphoregulator. Trends Cell Biol 17(1):44–50. doi:10.1016/j.tcb.2006.11.007
27. Ghajar CM, Blevins KS, Hughes CC, George SC, Putnam AJ (2006) Mesenchymal stem cells enhance angiogenesis in mechanically viable prevascularized tissues via early matrix metalloproteinase upregulation. Tissue Eng 12(10):2875–2888. doi:10.1089/ten.2006.12.2875
28. Ghajar CM, Chen X, Harris JW, Suresh V, Hughes CC, Jeon NL, Putnam AJ, George SC (2008) The effect of matrix density on the regulation of 3-D capillary morphogenesis. Biophys J 94(5):1930–1941. doi:10.1529/biophysj.107.120774
29. Brooks PC, Clark RA, Cheresh DA (1994) Requirement of vascular integrin alpha v beta 3 for angiogenesis. Science 264(5158):569–571
30. MacDonald TJ, Taga T, Shimada H, Tabrizi P, Zlokovic BV, Cheresh DA, Laug WE (2001) Preferential susceptibility of brain tumors to the antiangiogenic effects of an alpha(v) integrin antagonist. Neurosurgery 48(1):151–157
31. Liu Z, Wang F, Chen X (2008) Integrin alpha(v)beta(3)-targeted cancer therapy. Drug Dev Res 69(6):329–339. doi:10.1002/ddr.20265
32. Chen J, Green J, Yurdagul A Jr, Albert P, McInnis MC, Orr AW (2015) alphavbeta3 integrins mediate flow-induced NF-kappaB activation, proinflammatory gene expression, and early atherogenic inflammation. Am J Pathol 185(9):2575–2589. doi:10.1016/j.ajpath.2015.05.013
33. Nisato RE, Tille JC, Jonczyk A, Goodman SL, Pepper MS (2003) alphav beta 3 and alphav beta 5 integrin antagonists inhibit angiogenesis in vitro. Angiogenesis 6(2):105–119. doi:10.1023/B:AGEN.0000011801.98187.f2
34. Hompland T, Ellingsen C, Ovrebo KM, Rofstad EK (2012) Interstitial fluid pressure and associated lymph node metastasis revealed in tumors by dynamic contrast-enhanced MRI. Cancer Res 72(19):4899–4908. doi:10.1158/0008-5472.CAN-12-0903
35. Chary SR, Jain RK (1989) Direct measurement of interstitial convection and diffusion of albumin in normal and neoplastic tissues by fluorescence photobleaching. Proc Natl Acad Sci USA 86(14):5385–5389
36. Shin Y, Jeon JS, Han S, Jung GS, Shin S, Lee SH, Sudo R, Kamm RD, Chung S (2011) In vitro 3D collective sprouting angiogenesis under orchestrated ANG-1 and VEGF gradients. Lab Chip 11(13):2175–2181. doi:10.1039/c1lc20039a
37. Gerhardt H, Golding M, Fruttiger M, Ruhrberg C, Lundkvist A, Abramsson A, Jeltsch M, Mitchell C, Alitalo K, Shima D, Betsholtz C (2003) VEGF guides angiogenic sprouting utilizing endothelial tip cell filopodia. J Cell Biol 161(6):1163–1177. doi:10.1083/jcb.200302047
38. Gerhardt H (2008) VEGF and endothelial guidance in angiogenic sprouting. Organogenesis 4(4):241–246
39. Kim S, Lee H, Chung M, Jeon NL (2013) Engineering of functional, perfusable 3D microvascular networks on a chip. Lab Chip 13(8):1489–1500. doi:10.1039/c3lc41320a
40. Newman AC, Nakatsu MN, Chou W, Gershon PD, Hughes CC (2011) The requirement for fibroblasts in angiogenesis: fibroblast-derived matrix proteins are essential for endothelial cell lumen formation. Mol Biol Cell 22(20):3791–3800. doi:10.1091/mbc.E11-05-0393
41. Lee H, Kim S, Chung M, Kim JH, Jeon NL (2014) A bioengineered array of 3D microvessels for vascular permeability assay. Microvasc Res 91:90–98. doi:10.1016/j.mvr.2013.12.001
42. Sobrino A, Phan DT, Datta R, Wang X, Hachey SJ, Romero-Lopez M, Gratton E, Lee AP, George SC, Hughes CC (2016) 3D microtumors in vitro supported by perfused vascular networks. Sci Rep 6:31589. doi:10.1038/srep31589
43. Phan DT, Wang X, Craver BM, Sobrino A, Zhao D, Chen JC, Lee LY, George SC, Lee AP, Hughes CC (2017) A vascularized and perfused organ-on-a-chip platform for large-scale drug screening applications. Lab Chip 17(3):511–520. doi:10.1039/c6lc01422d
44. Sobrino A, Phan DT, Wang X, Datta R, Hachey SJ, López MR, Gratton E, Lee AP, George SC, Hughes CCW (2016) A vascularized and perfused human micro-tumor platform for cancer drug screening. SC Rep (in press)
45. Dreher MR, Liu W, Michelich CR, Dewhirst MW, Yuan F, Chilkoti A (2006) Tumor vascular permeability, accumulation, and penetration of macromolecular drug carriers. J Natl Cancer Inst 98(5):335–344. doi:10.1093/jnci/djj070
46. Nagy JA, Feng D, Vasile E, Wong WH, Shih SC, Dvorak AM, Dvorak HF (2006) Permeability properties of tumor surrogate blood vessels induced by VEGF-A. Lab Invest 86(8):767–780. doi:10.1038/labinvest.3700436
47. Vickerman V, Blundo J, Chung S, Kamm R (2008) Design, fabrication and implementation of a novel multi-parameter control microfluidic platform for three-dimensional cell culture and real-time imaging. Lab Chip 8(9):1468–1477. doi:10.1039/b802395f
48. Verbridge SS, Chakrabarti A, DelNero P, Kwee B, Varner JD, Stroock AD, Fischbach C (2013) Physicochemical regulation of endothelial sprouting in a 3D microfluidic angiogenesis model. J Biomed Mater Res A 101(10):2948–2956. doi:10.1002/jbm.a.34587

49. Nguyen DH, Stapleton SC, Yang MT, Cha SS, Choi CK, Galie PA, Chen CS (2013) Biomimetic model to reconstitute angiogenic sprouting morphogenesis in vitro. Proc Natl Acad Sci USA 110(17):6712–6717. doi:10.1073/pnas.1221526110
50. Chan JM, Zervantonakis IK, Rimchala T, Polacheck WJ, Whisler J, Kamm RD (2012) Engineering of in vitro 3D capillary beds by self-directed angiogenic sprouting. PLoS ONE 7(12):e50582. doi:10.1371/journal.pone.0050582
51. Li L, Wang L, Zhang W, Tang B, Zhang J, Song H, Yao D, Tang Y, Chen X, Yang Z, Wang G, Li X, Zhao J, Ding H, Reed E, Li QQ (2004) Correlation of serum VEGF levels with clinical stage, therapy efficacy, tumor metastasis and patient survival in ovarian cancer. Anticancer Res 24(3b):1973–1979
52. Galie PA, Nguyen DH, Choi CK, Cohen DM, Janmey PA, Chen CS (2014) Fluid shear stress threshold regulates angiogenic sprouting. Proc Natl Acad Sci USA 111(22):7968–7973. doi:10.1073/pnas.1310842111
53. Vickerman V, Kamm RD (2012) Mechanism of a flow-gated angiogenesis switch: early signaling events at cell-matrix and cell-cell junctions. Integr Biol (Camb) 4(8):863–874. doi:10.1039/c2ib00184e
54. Helm CLE, Fleury ME, Zisch AH, Boschetti F, Swartz MA (2005) Synergy between interstitial flow and VEGF directs capillary morphogenesis in vitro through a gradient amplification mechanism. Proc Natl Acad Sci USA 102(44):15779–15784. doi:10.1073/pnas.0503681102
55. Katsumi A, Orr AW, Tzima E, Schwartz MA (2004) Integrins in mechanotransduction. J Biol Chem 279(13):12001–12004. doi:10.1074/jbc.R300038200
56. Shamloo A, Xu H, Heilshorn S (2012) Mechanisms of vascular endothelial growth factor-induced pathfinding by endothelial sprouts in biomaterials. Tissue Eng Part A 18(3–4):320–330. doi:10.1089/ten.TEA.2011.0323